Numerical optimisation of the active lift turbines using OpenFoam's overset method

I. Robin[a*], D. Mouazé[a], A.-C. Bennis[a], G. Carpentier[b]

Abstract—**This study investigates the Active Lift Turbine, a new vertical-axis energy-collecting turbine through numerical simulations. The turbine utilises a unique crank-crank system to convert normal forces into momentum, thereby enhancing overall efficiency. To accurately model the non-circular blade trajectory within a two-dimensional computational domain, an overset method is employed. The study focuses on analysing three key parameters : blade incidence angle, turbine solidity parameter, and radial amplitude variation. The study in led using air for practical reasons but should be applicable to tidal turbines using a Reynolds similitude. The results obtained from the simulations demonstrate that the variation in radius alone leads to a decrease in power output. However, it is important to note that this power loss is primarily attributed to aerodynamic effects, which can be partially mitigated by adjusting the solidity parameter. Consequently, the sizing requirements for active lift turbines differ from those of the conventional Darrieus turbines. Additionally, the study highlights the potential for active control of the incidence angle to further enhance turbine performance. By actively manipulating the angle, it becomes possible to optimize the turbine's response to varying flow conditions. Furthermore, the flow in the wake of the active lift turbine shows less symmetrical characteristics compared to a classical Darrieus turbine, offering an opportunity to improve the average efficiency of two coupled turbines.**

Index Terms—**Active Lift Turbine, Turbine optimisation, Overset, Renewable Energy...**

I. Introduction

In the last decades, efforts to optimise energy recovery turbines have mainly focused on Horizontal Axis Turbines (HAT) [1]. They generally have a higher efficiency and allow for the installation of larger industrial-scale power plants especially for off-shore sites. However, with the emergency for energy transition comes the need to consume energy where it is produced to limit the losses by Joule effect. Vertical Axis Turbines (VAT) are generally less efficient than HAT. However, they are less expensive to produce because they operate with a direct drive system and therefore do not require a gearbox between the rotor and the generator (in most cases). Their level of complexity is generally lower, as for the blades that are often straight. Smaller, they are better suited to multi-directional, low intensity and turbulent flows than HATs. There wind version are therefore ideal for urban or harbour areas where energy is locally consumed. The difference in efficiency between HAT (40-50%) and VAT (30-40%) can be explained by the higher interaction between the blades for VAT. Also, during rotation, the blades of a VAT are not always facing the flow, and their aerodynamic performance depends on their position on their rotation. But HATs alone is not suitable for all configurations and VAT optimization becomes more important. Abandoned at the end of the 1980s, a better understanding of the effect of fatigue loading has allowed a resurgence of research on VAT since 2005 [2]. The parametric studies so far applied to HATs are taken up for application to VATs. This is especially the case for the parametric studies on Tip Speed Ratio, foil and blade shape, rotor size and turbulence [3]–[8]. However, the effects of these parameters are quite different depending on the technology. For example, for TSR, the peak efficiency is more like 7 to 8 for HATs. It is much lower for VATs, and is rather between 2 and 4 depending on the geometry of the turbine [9], [10]. For blade shapes, studies on blade twisting are relatively widespread for HATs. This process allows the angle of attack of the foil to be adapted to its distance from the rotor and the speed of rotation [11]. This kind of deformation does not make sense for a VAT (where the distance of the foil from the rotor does not vary with height), but the blades are sometimes deformed or tilted to help the turbine start at low flow speeds (by shifting the foil according to height) [12]. Other parameters are specific to VATs and introduced to describe their specificity. For example, [13] show that the aspect ratio of the projected surface (h/R, with h and R the turbine's height and radius, respectively) of the turbine plays an important role in the calculation of its power coefficient. Turbines that are wider than they are tall have higher efficiency than those with an aspect ratio close to 1 for equal swept areas (hR). The solidity (Nc/R, where N is the number of blades, and c the foils chord) of the turbine also seems to play a predominant role in the sizing of VATs. This geometrical parameter directly impacts the operating range of the turbine and its optimal C_p (P_{out}/P_{in}, where P_{out} is the power collected by the turbine and P_{in} is the dynamic power contained in the flow). For example, with a solidity of 0.1, the operating range of the turbine is a TSR between 3.5 and 5, while with a solidity of 0.35, the optimum is expected to be a TSR between 2 and 3.5

The authors thank the regions of "Normandie" and "Île-de-France" as well as "Vallée de la Seine", but also ADEME for their financial support. The independence of the results from the interests of the founders is assured thanks to their investments.

a. Normandie Univ, UNICAEN, CNRS, UNIROUEN, Morphodynamique Continentale et Cotière (M2C), Caen, France
b. Builders - École d'Ingénieur, Engineering School, Caen, France.
∗ corresponding author : ilan.robin@unicaen.fr

The authors are grateful to the CRIANN for calculation facilities and technical support.

Digital Object Identifier: https://doi.org/10.36688/ewtec-2023-209

[9]. The impact of blade angle on efficiency is also often studied. Depending on the blade profile chosen, it can improve or deteriorate the C_p by a few percent [8], [14], [15] and can be implemented with a simple, passive mechanical system. The axis around which the profile rotates to control its incidence (mounting position) is also a commonly studied parameter [16]. All these studies, advances and benchmarks have resulted in VAT efficiency of around 40%. However, the difference in efficiency between HAT and VAT is still about 10%, still far from the Betz limit (59%) [17]. This observation shows that it is still possible to extract more power from the fluid with VATs. Thus, a recent study shows that the average efficiency of VATs could be increased by 15% if they were positioned in the right way in relation to each other [18]. This turbine coupling method is effective, but does not appear to be suitable for an urban environment. At the scale of a single turbine, new concepts are gradually emerging. The Active Lift Turbine (A.L.T.) is one of them (Patent EP2183479 [19]). This work aims to better understand and improve the A.L.T. concept. This work is done in the frame of the Green River Project that aims to build a floating multi-sources electric hub. The prototype includes the presentation of two A.L.T.: a wind turbine and a tidal turbine. For reasons of simplification and access to the physical equipements, this study focuses on a wind turbine. However, the results should be easily applicable to a tidal turbine using Reynolds similarity. The full-scale floating platform is located in an estuarine area. The tidal turbine is therefore subject to the effects of tides and river currents.

After a short introduction, Section II describes the method used by detailing the specificity of A.L.T., the numerical setup, and the studied parameters. The results are presented in Section III. The different parameters are changed to measure their impact on the C_p and normal forces to compare their net power and the potential of additional power. The conclusion (Section IV) sums up the results and defines the research trajectory for future works.

II. Methodology

This study is entirely numerical. A mesh convergence study was previously performed on a known Darrieus tidal turbine [20]. This work keeps the same ratio $\Delta x/c$ where δx is the characteristic length of cells in the mesh. The simulation results were compared with the experimental results and show an overestimation of the C_p by a maximum of 5%.

A. Active lift turbine description

The A.L.T. is a concept that aims improve the performances of VAT. Its principle is based on the observation that, based on Betz theory, there is necessarily a part of the energy contained in the fluid that is still to be collected. Thus, by deforming the trajectory of the blades, the A.L.T. collects, in addition to the usual torque, part of the normal forces that apply to the turbine. These forces, coupled with a radial displacement guaranteed by a connecting rod-crank system, produce additional power. Currently, the generic equation for the blade trajectory can be written as :

$$R(\theta) = R_{max} - f(\theta), \tag{1}$$

where θ is the position angle, R is the distance between a blade and the center of rotation, R_{max} is the maximum radius of the turbine and $f(\theta)$ is a periodic function. In this work,

$$f(\theta) = B\sin^2\theta, \tag{2}$$

where $B \in [0, R_{max}[$ is the radial magnitude coefficient with B. Note that with $B = 0$, the blades follow a classic Darrieus trajectory.

The physical parameters of the reference turbine are given in Table I.

TABLE I
SUMMARY OF THE PHYSICAL PARAMETERS USED IN DYNAMIC SIMULATIONS OF THE ROTOR IN THE REFERENCE CASE

Parameter	Value
Blade profile	BS120
Number of blades	3
Radius max (R_{max})	0.55 m
Radial variation amplitude (B)	0.07 m
Chord (c)	0.12 m

The blades profile (BS120) is usually used as sunshade for buildings. It is produced in industrial scale, is easier to find and less expensive than NACA profiles. It is a symmetrical profile with bulges on its middle (Fig. 1).

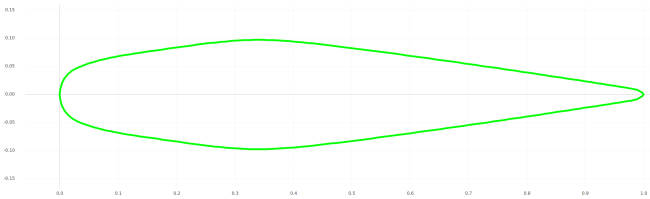

Fig. 1. Dimensionless BS120 profile

The blade number and the chord length are chosen according to [9] to assure the sizing of the Darrieus turbine.

B. Numerical setup

1) Fluid properties and motion: In this work, the inlet flow velocity (U_∞), the maximum radius (R_{max}) and the rotational speed (Ω) are constant. The Tip Speed ratio (TSR or $\lambda = \frac{\Omega R_{max}}{U_\infty}$) is therefore constant as well and equal to 2.5. The fluid properties are summed up in Table II. The flow characteristics (flow velocity and flow turbulence rate) are chosen according to the potential implantation site of the turbine.

TABLE II
SUMMARY OF THE FLOW PROPERTIES

Parameter	Value	Unit	Description
ρ	1.225	$\mathrm{kg{\cdot}m^{-3}}$	Air density
ν	1.5×10^{-5}	$\mathrm{m^2{\cdot}s^{-1}}$	Kinematic viscosity
U_∞	8	$\mathrm{m{\cdot}s^{-1}}$	Flow inlet velocity
I	5%	-	Turbulence rate

The maximal relative velocity of the blades can be computed as

$$U_{rel} = \Omega \cdot R_{max} + U_\infty = 28 \text{ m.s}^{-1}. \quad (3)$$

The Mach number is given by

$$Ma = U_{rel}/a = 28/340 = 0.08, \quad (4)$$

where a is the sound velocity in air. As $Ma << 0.3$, the fluid (air) is supposed to be incompressible. This hypothesis is valid in the water for the equivalent tidal turbine. Gravity and ground effects (flow velocity already includes ground effects) are neglected. The fluid is also considered as viscous and thus, the continuity Navier-Stokes equation is solved using the bi-dimensional finite volume method :

$$\frac{\partial u_i}{\partial x_i} = 0, \quad (5)$$

where u is the fluid velocity and $i = 1, 2$. The motion conservation equation is solved in the same condition such that

$$\frac{\partial u_i}{\partial t} + \frac{\partial u_i u_j}{\partial x_j} = -\frac{1}{\rho}\frac{\partial p}{\partial x_i} + \nu \frac{\partial^2 u_i}{\partial x_j \partial x_j} + \frac{1}{\rho} f_i, \quad (6)$$

where t is the time, p is the pressure and f are external forces.

2) Mesh and blades motion: The computational domain extends 7 R_{max} upstream and 10 R_{max} downstream the center of rotation (located in (0,0)). It is 14 R_{max} wide. A refinement tore is made around the blade trajectory ($R_{max} \pm 2B$) using the OpenFoam meshing tool, snappyHexMesh.

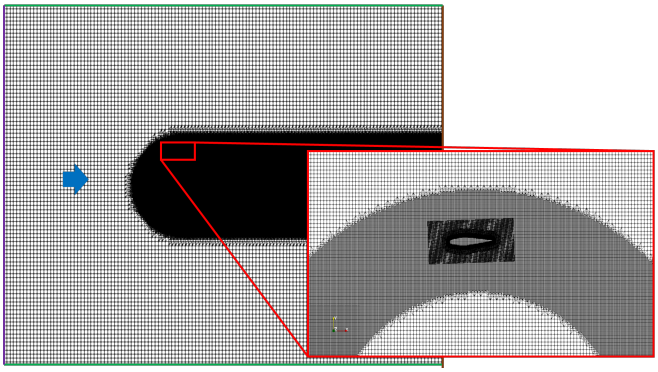

Fig. 2. Overall mesh of the computational domain. The blue line represents the inlet velocity condition, the green lines the lateral slip conditions and the brown line the pressure gradient outlet condition. The blue arrow is to show the flow direction and the red squares are a zoom on the mesh close to the turbines blade.

The most commonly used method for modelling blade motion is the Arbitrary Mesh Interface (AMI). It separates the computational domain into a fixed and a rotating domain and transfers the fluid characteristics from one to the other. To model the blade trajectory of the A.L.T., it could theoretically be coupled with a mesh deformation module. However, B can be a large variation and involve large mesh deformation, which can lead to numerical instabilities. Re-meshing implies an excessive computational cost. The method chosen to model the A.L.T. is therefore the overset method. It is the superposition of two meshes. The background mesh, constituting the calculation domain, and the mobile meshes (one per blade) whose displacement is prescribed. The mesh around a blade is shown in Fig. 3.

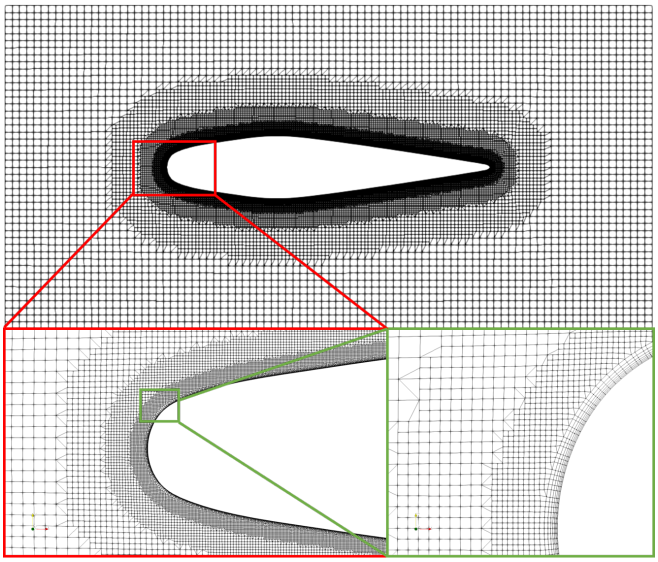

Fig. 3. Overset mesh around the blade with two zooms (red and green boxes)

The fluid characteristics are interpolated to two positions for all iterations of the solver (pimpleFoam) using a inverse distance interpolation scheme. First at the edge of the overset mesh where the fluid characteristics from the background mesh are interpolated to be used as boundary conditions for the overset. Secondly, close to the blades where the result of the fluid calculation in the overset is fed back into the background mesh, as if it were a special wall condition Fig. 4.

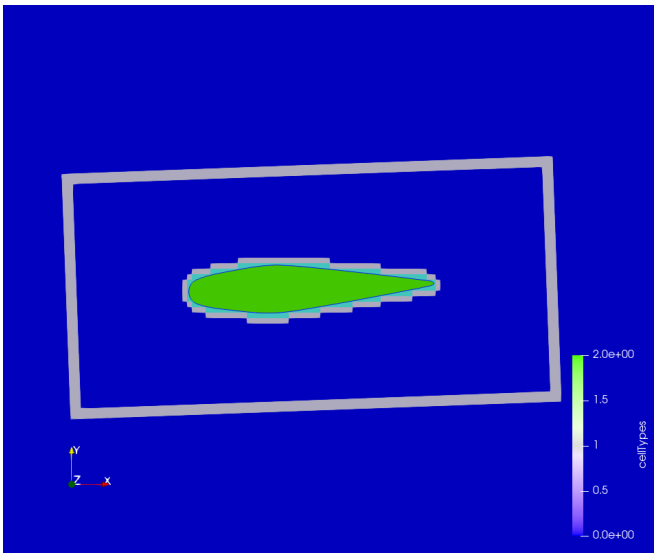

Fig. 4. Cell type around the blades. Dark blue cells are calculated using the fluid model in background and overset meshes, light blue cells are only calculated in the overset mesh and green cells are not calculated. Grey cells are the interpolating cells

The complete mesh has 438 000 calculation cells including the 43 000 of each overset around the blades. The maximum of cells aspect ratio is 8.9 and is located

on the 740 cells on each blade surface because they are longer than thick. Mean aspect ratio is 1.3. The minimum cell volume is $1.18.10^{-10}$m and the max skewness is 0.87.

The movement of the blades is forced by a constant rotation speed condition and is described independently for each blade. It is provided to OpenFoam as a time series of displacement relative to the initial position of each overset. At $t = 0$, the oversets are respectively at 0°, 120° and 240° at a distance $R_0 = R_{max}$ from the centre of rotation (0,0,0). At the time $t + \delta t$ (where δt is an infinitesimal time step), each blade must be put back on its trajectory (in the case where $f = Bsin(\theta)$, the blade at 0° is already on its trajectory but not the two others). This displacement is large and sudden (Fig. 5). It is the source of strong numerical divergences in the calculation if it is not correctly treated. To put the blades back on their trajectories, OpenFoam runs for an iteration without fluid (moveDynamicMesh function). Thus, the blades are put back on their trajectory and their motion can be described using a single equation (instead of having to adapt R_0).

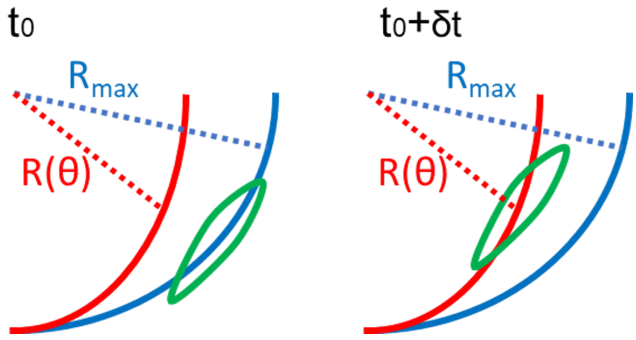

Fig. 5. Correction at initialisation in order to put the blades on their trajectories.

C. Parametric study

1) Radial magnitude coefficient B: B is a coefficient specific to the A.L.T.. The previous comparison of a Darrieus turbine with an A.L.T. revealed that the particular displacement of the blades of the A.L.T. leads to a degradation of the net C_p but also to an increase of the normal forces. Varying the B parameter may reveal an optimum between torque loss and increased normal forces (converted by the crank rod system). Three values of B are therefore compared: 0 (Darrieus), 0.033 and 0.07 (reference). The three blade trajectories are plotted on Fig. 6.

2) Solidity parameter σ: As explained in Section I, the solidity parameter should be taken into account when dimensionning a VAT. The impact on performances of the turbine according to σ is quite well known for Darrieus turbine but its has never been studied for A.L.T.s. Leverages to change σ are c, N and R_{max}. Changing R_{max} of the turbine requires to change the flow inlet velocity to maintain a constant λ. Changing N, the number of blades requires to introduce new blades in the mesh (overset) as well as new equations for the displacement of each of them. This operation is

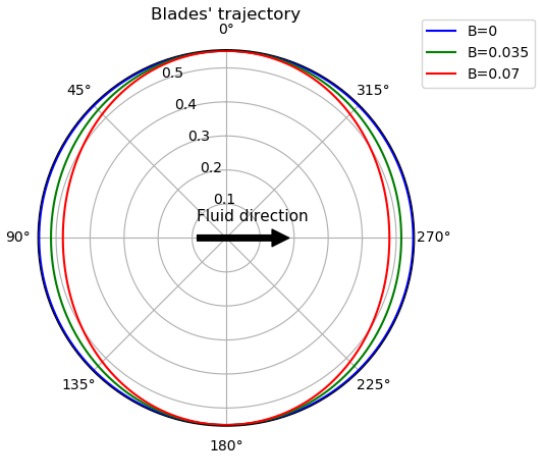

Fig. 6. Blades trajectory according to B. The blue circle is the Darrieus turbine. The green and red lines are for A.L.T with respectively $B = 0.035$ and $B = 0.070$

time consuming. Thus, changing the chord seems to be the simplest way to vary σ. However, this modification changes the Reynolds of the flow "seen" by the profile ($Re_c = U_\infty c/\nu$). For a classic Darrieus turbine, the optimal solidity for a turbine with a $\lambda = 2.5$, is $\sigma \approx 0.33$. This value is the reference value. Previous results show that the optimum operation of the A.L.T. is achieved for a higher λ at constant solidity. Four other values of σ are tested ($\sigma = 0.23$, $\sigma = 0.28$, $\sigma = 0.38$,$\sigma = 0.43$) to see if the behaviour of the A.L.T. according to this parameter is similar to the Darrieus one.

3) Incidence (β) control: Each profile has an optimal angle of incidence to increase its lift. For a chord of 0.12 m, $Re_c = 2.24 \times 10^5$. In steady state, XFoil gives an optimal angle for lift coefficient at 12° for BS120 (Fig. 7).

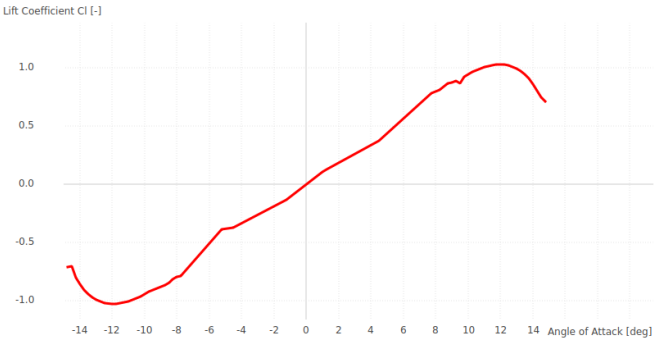

Fig. 7. Lift Coefficient against the angle of attack of a BS120 according to XFoil

The first variation of the reference case is done with a constant $\beta = \beta_{opti} = 12°$(0.21 radian).

A.L.T. already revealed some dynamic stall in the S-W quarter of the rotation (90°-180°). This phenomenon was not found for the equivalent Darrieus turbine. It is due to the modification of the angle of attack (the angle between the line of the chord of the blade and the relative flow) due to the radius variation. For a Darrieus VAT, the angle of attack is given by :

$$\alpha(\theta) = -\arctan\left(\frac{\sin\theta}{(\lambda+\cos\theta)}\right). \quad (7)$$

Thus, the incidence angle of the second case was defined as :

$$\alpha(\theta) + \beta = \beta_{opti}. \quad (8)$$

This choice is made in order to reduce the angle of attack of the blades on the complete rotation. The Fig. 8 shows the evolution of β against the position angle for this case.

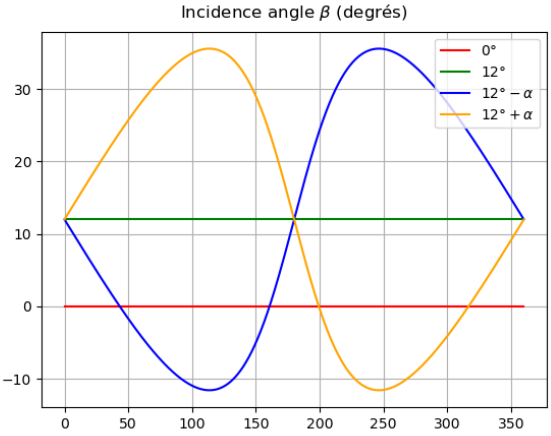

Fig. 8. Incidence angle for the different cases. The red line is the reference case with a 0° incidence angle, the green line is the case #7 with a constant 12° incidence angle. The blue and yellow lines show #8 and #9 cases with β depending on θ.

The input files describing the motion of the blades in OpenFoam contain two types of displacement: translation and rotation. All these displacements must be described with respect to a fixed point in the domain (the simplest being (0,0)). This constraint implies that the control of the angle of incidence must be introduced as a rotation (around the z-axis), in the same way as the rotation that makes the blade turn around (0,0). The introduction of a variable incidence angle *de facto* modifies the position of the blade in its rotation trajectory. This error must be corrected by means of translations (Fig. 9). In a cylindrical coordinates system the correction vector $\overrightarrow{AB}$ is therefore :

$$\overrightarrow{AB} = \overrightarrow{R}(\theta) - \overrightarrow{R}(\theta - \beta(\theta)) \quad (9)$$

TABLE III
SUMMARY OF ALL CASES

Name	B	σ	β
Ref	0.07	0.33	0°
#1	0	0.33	0°
#2	0.035	0.33	0°
#3	0.07	0.23	0°
#4	0.07	0.28	0°
#5	0.07	0.38	0°
#6	0.07	0.43	0°
#7	0.07	0.33	12°
#8	0.07	0.33	12°−$\alpha(\theta)$
#9	0.07	0.33	12°+$\alpha(\theta)$

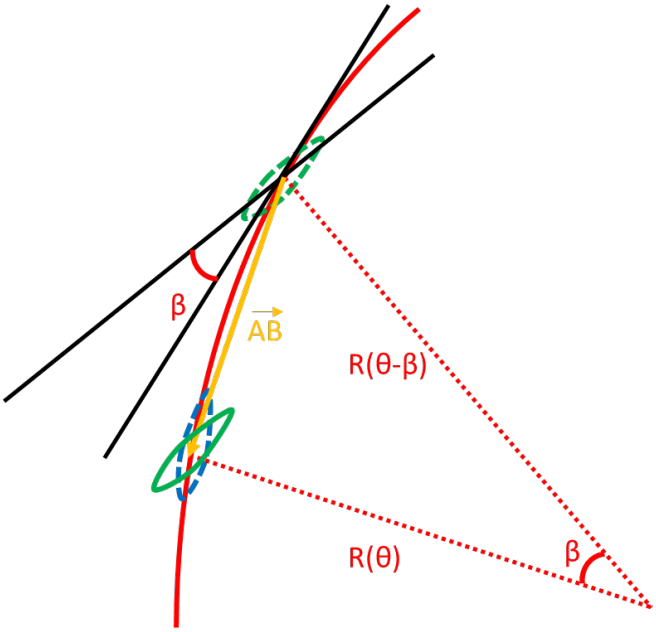

Fig. 9. Scheme explaining the mandatory correction of the incidence angle. The blade in blue without the incidence angle is located $R(\theta)$. When imposing the incidence angle, the blade moves back (green dotted line). A translation correction $\overrightarrow{AB}$ is applied (orange arrow). The final position of the blade is the green plain line.

III. Results

The model is run on five full rotations. The first round is not kept because it is too affected by the initialisation of the calculation. Results are presented on a full rotation. The power coefficient and the normal forces are chosen as representative values for the turbines performances. In this part, the power is only derived from the calculated moment on the blades ($P_{out} = \sum M\Omega$, where M is the moment). The power coefficient C_p therefore does not include the additional forces that could potentially be recovered by the A.L.T. To assess this additional energy, the normal forces are also monitored and compared. Normal forces are computed as

$$\overrightarrow{N} = \sum_{blades} \overrightarrow{F}.\frac{\overrightarrow{R}(\theta)}{R(\theta)}, \quad (10)$$

where $\sum_{blades} \overrightarrow{F}$ is the overall forces on the blades.

To ease the description of the results, the rotation is divided in quarters : Nord-West (N-W) between 0° and 90°, South-West (S-W) between 90° and 180°, South-East (S-E) between 180° and 270° and North-East (N-E) between 270° and 360°.

A. Impacts of the radial magnitude coefficient B

Figure 10 shows the the evolution of the C_p for the complete turbine on a full rotation for the different values of B.

The introduction of the radius variation leads to a general decrease in C_p but an increase in the amplitude of its variations (up to 20%). The power, and in particular the extremums, also shows a phase shift proportional to B (7° for B=0.07). The downward shift in C_p values implies that the turbine goes through

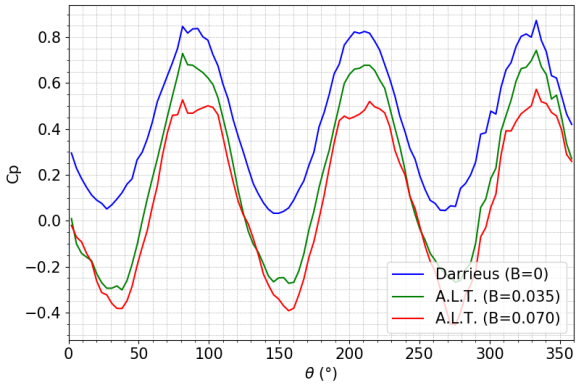

Fig. 10. Evolution of total C_p according to the position θ for different B-values

regimes where it is no longer driving but consuming energy (0-50°, 125-175° and 250-300°). This is a problem for VATs as this phenomenon creates positions where the turbine can block itself. The power generated by an isolated blade over one rotation is plotted in Fig. 11 to better understand the origin of this power loss.

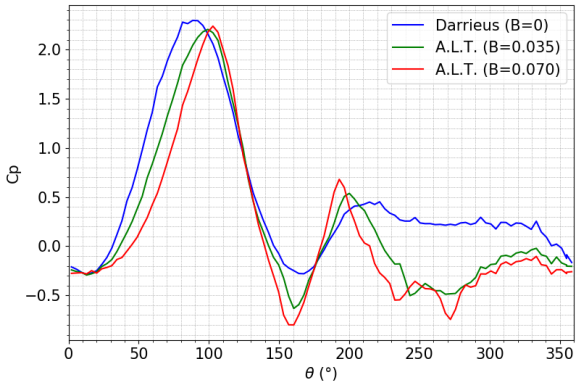

Fig. 11. Evolution of one blade C_p according to the position θ for different B-values

In all cases, the power peak is located on the upstream part of the rotation (30-130°). This is followed by a significant power loss between 135 and 180°. This negative moment is much more pronounced on the A.L.T. (-0.6 of minimum Darrieus C_p). The behaviour of the turbine really diverges beyond 200°. The power generation remains low but positive for the Darrieus but collapses for the A.L.T..

This dynamic is due to the behaviour of the fluid around the blades at different positions on the trajectory. Under the study conditions, all three turbines show vortex releases around 160°, indicating aerodynamic stall (Fig. 12). This is not specific to the A.L.T. as it also exists in the simulation with B=0 (Darrieus). On the other hand, this turbine braking is accentuated for the A.L.T.. In addition, most of the power is lost in the second half of the rotation, from 200°. On this part of the rotation (200-360°), the approach of the turbine to its centre of rotation causes the moment to fall without compensating it by an increase in aerodynamic forces. Here again, the blade shows signs of significant vortex release.

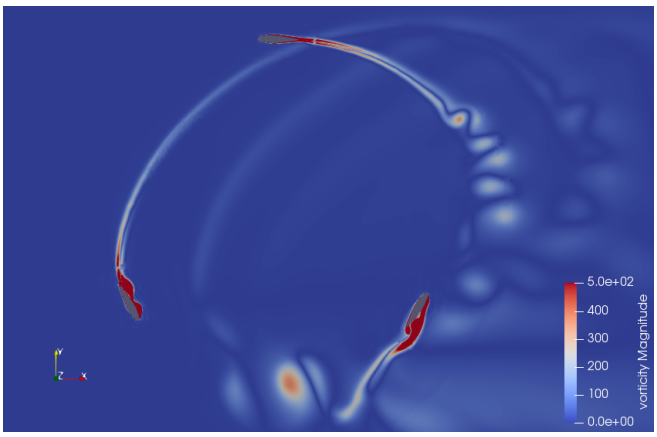

Fig. 12. Vorticity field of the A.L.T. with B=0.07 and $\sigma = 0.33$

The A.L.T. changes the interaction between the blades and the flow in two ways. First, at constant rotational speed, the blade undergoes consecutive acceleration and deceleration phases due to the radius variation. Secondly, the angle of attack of the foil is changed compared to the full rotation of a Darrieus turbine. Both effects increase the complexity of the system and highlight the impossibility of handling and optimising A.L.T. like Darrieus.

For normal forces, the results show a 25% increase between the Darrieus and the A.L.T. with $B = 0.07$. Considering the turbine as a whole, the values of the maximums are close. However, the minimums are higher for the A.L.T. (Fig. 13). Note that the values of the normal forces are dependent on the flow characteristics. In water, the values of these forces are expected much higher because of the water density. For a single blade, there is a delay in the normal upstream force peak. This is expected because from 0° to 90°, the blades move closer to the centre of rotation and therefore backwards in relation to the flow. But after 90°, the blades move away again and this movement leads to the increase of the normal forces to a similar intensity as the Darrieus. In the East, the Darrieus turbine shows a symmetrical behaviour between North and South with a minimum at 270° while the A.L.T. shows an increase of the normal forces before 270° but a decrease afterwards. This time, the phenomenon can simply be explained by the radial movement of the blade. The reduction in amplitude of the normal force is not necessarily beneficial to the A.L.T. which can collect it in compression and extension.

The distribution of the velocity field across the A.L.T. is also asymmetric (Fig. 14). The flow to the north is accelerated while the flow to the south is strongly slowed down. This phenomenon is to the advantage of the A.L.T. as it should allow the increase of the efficiency of two twin contra-rotating turbines.

B. Impacts of the solidity σ

The chord of the reference turbine is sized to optimise the equivalent Darrieus turbine according to

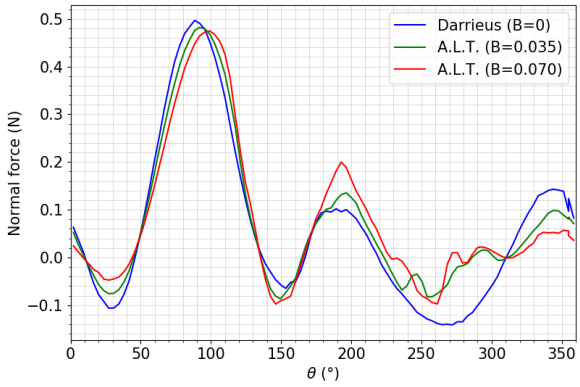

Fig. 13. Evolution of normal force according to the position θ for different B-values

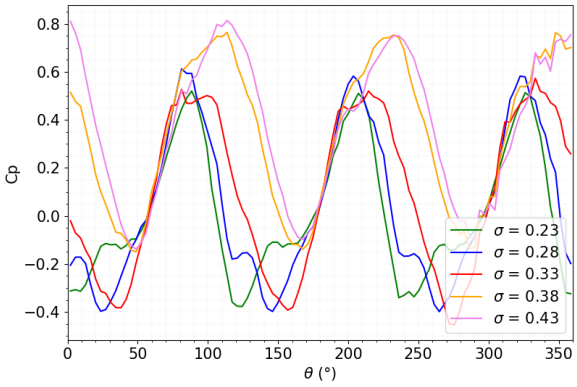

Fig. 15. Evolution of total C_p according to the position θ for different σ-values

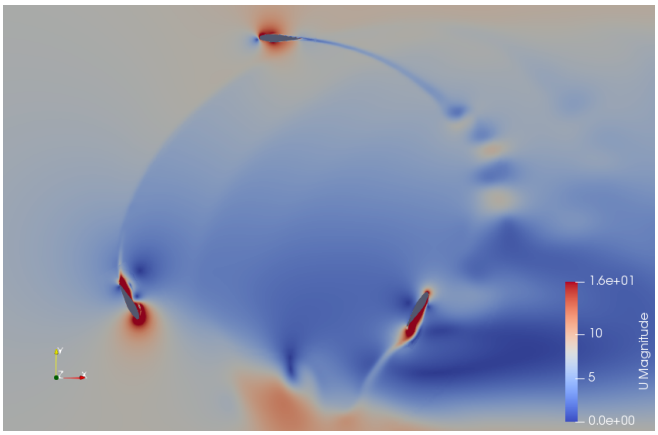

Fig. 14. Velocity field around the A.L.T. for $B = 0.07$ and $\sigma = 0.33$

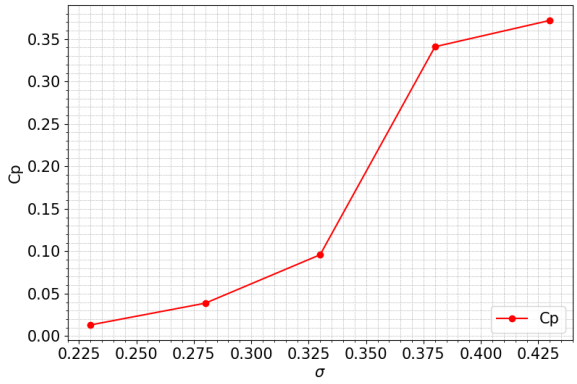

Fig. 16. Evolution the C_p according to σ for $B = 0.07$

[9]. However, as shown in Section III-A, much of the available energy is lost for aerodynamic reasons. The blades of the A.L.T. stall due to variations in speed and angle of attack during it's rotation. Changing the solidity parameter by changing the chord is equivalent to modifying the Re_c "seen" by the blades. The trend is consistent for the tested values of solidity. As the chord increases, the amplitude of variation of C_p increases as well as its mean value (Fig. 15 and 16). The power extremes are also out of phase by a few degrees (4° for 15% of σ).

This phenomenon is more visible on the plots of an isolated blade (Fig. 17). The phase shift at the maximum power position of the turbine is about 7% for a variation of σ of 15%. The generator operating range of the turbine increases from 50-130° for $\sigma = 0.28$ to 50-150° for $\sigma = 0.38$ upstream and from 180-210° to 180-300° downstream. For $\sigma = 0.38$, the power curve approaches that of the Darrieus at $\sigma = 0.33$. The range of operation in generator mode remains less extensive, especially on the northern part of the rotation (270-90°).

Increasing the chord partially avoids aerodynamic stall in the East part of the rotation (Fig. 18). For $\sigma = 0.38$, the N-E section is still not generating power even though the boundary layer is attached. The vortexes release in the south section are still present and correspond to the drop of power around 160°.

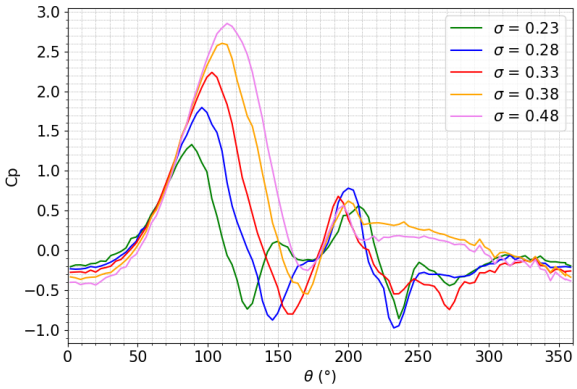

Fig. 17. Evolution of one blade C_p according to the position θ for different σ-values

C. Impacts of the incidence angle

All tested incidence control scenarios lead to a drastic degradation of Cp and A.L.T. normal forces (Fig. 19). The aerodynamic stall generates strong turbulence in the flow. The scenario choices are not suitable.

The loss of power is mainly located to the West in the first half of the rotation. It should be noted, however, that over the second half, a power peak around 250° is observed and the average C_p over this section is 14% higher. Even if the choice of this angle

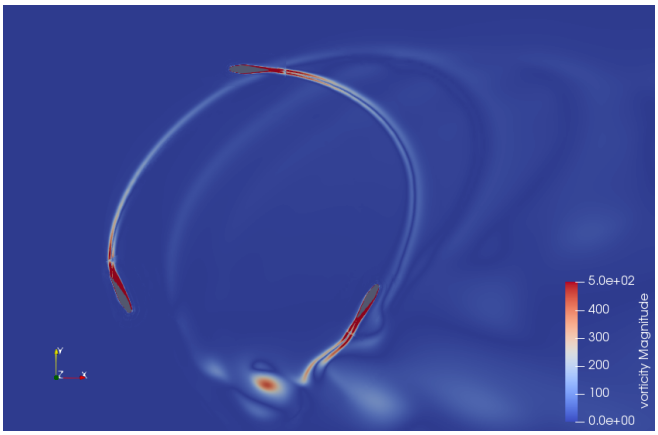

Fig. 18. Vorticity field around the A.L.T with $B = 0.07$ and $\sigma = 0.38$

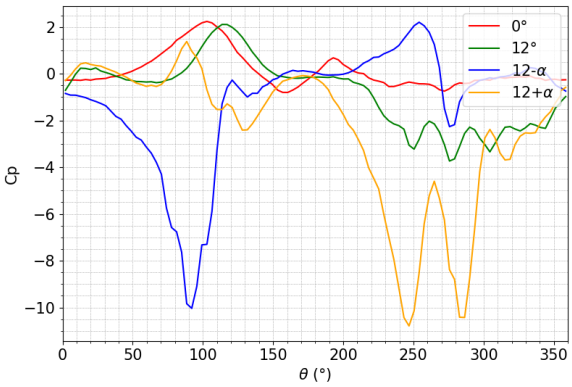

Fig. 19. Evolution of one blade C_p according to the position θ for the different scenario for the incidence angle β.

of incidence control does not seem to have been the most appropriate, the control of the angle of incidence seems to play a primordial role in the optimisation of the A.L.T.

IV. Conclusion

In this work, the impact on the performance of three parameters, characteristic of vertical axis turbines, is investigated for an innovative type of turbine called Active Lift Turbine. This research is carried out using only a numerical approach with the OpenFoam code and its overset module. This module is particularly suited to complex movements of structures.

The first parameter is the B-coefficient, specific to A.L.T., which strongly deteriorates the Cp of the turbine when introduced alone. This is due to the influence of this parameter on the dynamics (acceleration and deceleration) and the angle of attack of the blades.

The introduction of the radial variation induces, among other things, an aerodynamic stall on the southern part of the rotation.

The second parameter is solidity, which is a geometric parameter of the turbine. It acts on the Re_c. The results of this work show that the increase in blade chord compensates for some of the power losses due to the introduction of B. In fact, the change in blade trajectory does not allow the A.L.T. to operate with the same characteristics as a Darrieus. A Cp of 34% is observed for a couple $(B, \sigma) = (0.07, 0.38)$ whereas a turbine whose only parameter B has been modified shows a very high power loss ($C_p \approx 9.5\%$). This observation is encouraging for the further optimization of the turbine because if high Cps can be reached again with a B coefficient large enough to have a radial displacement, the technology is likely to significantly improve the efficiency of VATs. For this to happen, further studies will have to be carried out. First of all, the concept must be physically validated. Then, numerically, new heat maps of Cp will have to be made, specifically for the A.L.T.. They will have to include, at least, B, σ and λ.

In this work, a control of the angle of incidence is also introduced. However, it turned out to be unsuccessful. The power coefficient drastically dropped after introducing an incidence angle. This failure can be explained in different ways. After consideration, the chosen "optimal" angle (β_{opti}) is probably too large. This is taken to maximise the lift of the foil, but in the case of a turbine, the lift/drag ratio takes precedence. Further attempts should be made in this direction. Furthermore, in this work, the angle of attack was calculated without taking into account the angle variations linked to the radial variation. The angle of attack should instead be written as :

$$\alpha(\theta) = -\arctan\left(\frac{-f'/U_\infty + \sin\theta}{(\lambda + \cos\theta)}\right), \qquad (11)$$

where f'= is the first derivative of f.

Fixed and varying angles should be tested but with a more progressive approach. Note that varying angles implies a more complex mechanical system. If the aerodynamic efficiency is not significantly improved by such a system, it won't compensate its mechanical losses.

Lastly, as the A.L.T. seems to make the velocity field asymmetric, it would be interesting to carry out a study of a coupling of two spatially shifted A.L.T.

The study of active lift turbines is still in its beginning, but this work provides clues on the parameters that could be investigated and optimised. It has also led to the development of number of well suited tools for the study of these turbines. Similar studies using water instead of air should also be done in order to confirm the independence of the results from the fluid characteristics. They might be coupled with experimental results of the physical turbine of the Green River Project.

Acknowledgement

Thanks to P. Lecanu (Patent EP2183479 [19]) for allowing us to work on his under patent turbine concept. Authors thanks P. Robin for English reviewing.

References

[1] I. Yahyaoui and A. S. Cantero, "Chapter 16 - modeling and characterization of a wind turbine emulator," in *Advances in Renewable Energies and Power Technologies*, I. Yahyaoui, Ed. Elsevier, 2018, pp. 491–508. [Online]. Available: https://www.sciencedirect.com/science/article/pii/B9780128129593000162

[2] B. Hand and A. Cashman, "A review on the historical development of the lift-type vertical axis wind turbine: From onshore to offshore floating application," *Sustainable Energy Technologies and Assessments*, vol. 38, p. 100646, 2020. [Online]. Available: https://www.sciencedirect.com/science/article/pii/S2213138819309075

[3] Q. Cheng, X. Liu, H. S. Ji, K. C. Kim, and B. Yang, "Aerodynamic analysis of a helical vertical axis wind turbine," *Energies*, vol. 10, no. 4, 2017. [Online]. Available: https://www.mdpi.com/1996-1073/10/4/575

[4] A. Subramanian, S. A. Yogesh, H. Sivanandan, A. Giri, M. Vasudevan, V. Mugundhan, and R. K. Velamati, "Effect of airfoil and solidity on performance of small scale vertical axis wind turbine using three dimensional cfd model," *Energy*, vol. 133, pp. 179–190, 2017. [Online]. Available: https://www.sciencedirect.com/science/article/pii/S0360544217308757

[5] M. F. Ismail and K. Vijayaraghavan, "The effects of aerofoil profile modification on a vertical axis wind turbine performance," *Energy*, vol. 80, pp. 20–31, 2015. [Online]. Available: https://www.sciencedirect.com/science/article/pii/S0360544214012894

[6] M. S. Siddiqui, A. Rasheed, T. Kvamsdal, and M. Tabib, "Effect of turbulence intensity on the performance of an offshore vertical axis wind turbine," *Energy Procedia*, vol. 80, pp. 312–320, 2015, 12th Deep Sea Offshore Wind RD Conference, EERA DeepWind'2015. [Online]. Available: https://www.sciencedirect.com/science/article/pii/S1876610215021670

[7] D. Grogan, S. Leen, C. Kennedy, and C. O'Bradaigh, "Design of composite tidal turbine blades," *Renewable Energy*, vol. 57, p. 151–162, 09 2013.

[8] N. Kolekar, S. Mukherji, and A. Banerjee, "Numerical modeling and optimization of hydrokinetic turbine," 01 2011.

[9] A. Rezaeiha, H. Montazeri, and B. Blocken, "Towards optimal aerodynamic design of vertical axis wind turbines: Impact of solidity and number of blades," *Energy*, vol. 165, pp. 1129–1148, 2018. [Online]. Available: https://www.sciencedirect.com/science/article/pii/S0360544218319704

[10] R. C. Maydew and P. C. Klimas, "Aerodynamic performance of vertical and horizontal axis wind turbines," *Journal of Energy*, vol. 5, no. 3, pp. 189–190, 1981.

[11] H. K. Nejadkhaki, A. Sohrabi, T. P. Purandare, F. Battaglia, and J. F. Hall, "A variable twist blade for horizontal axis wind turbines: Modeling and analysis," *Energy Conversion and Management*, vol. 248, p. 114771, 2021. [Online]. Available: https://www.sciencedirect.com/science/article/pii/S019689042100947X

[12] R. Kumar, K. Raahemifar, and A. S. Fung, "A critical review of vertical axis wind turbines for urban applications," *Renewable and Sustainable Energy Reviews*, vol. 89, pp. 281–291, 2018. [Online]. Available: https://www.sciencedirect.com/science/article/pii/S1364032118301254

[13] S. Brusca, R. Lanzafame, and M. Messina, "Design of a vertical-axis wind turbine: how the aspect ratio affects the turbine's performance," *International Journal of Energy and Environmental Engineering*, vol. 5, pp. 1–8, 08 2014.

[14] M. M. Elsakka, D. B. Ingham, L. Ma, and M. Pourkashanian, "Cfd analysis of the angle of attack for a vertical axis wind turbine blade," *Energy Conversion and Management*, vol. 182, pp. 154–165, 2019. [Online]. Available: https://www.sciencedirect.com/science/article/pii/S0196890418313980

[15] M. T. Nguyen, F. Balduzzi, and A. Goude, "Effect of pitch angle on power and hydrodynamics of a vertical axis turbine," *Ocean Engineering*, vol. 238, p. 109335, 2021. [Online]. Available: https://www.sciencedirect.com/science/article/pii/S0029801821007526

[16] M. M. Elsakka, D. B. Ingham, L. Ma, M. Pourkashanian, G. H. Moustafa, and Y. Elhenawy, "Response surface optimisation of vertical axis wind turbine at low wind speeds," *Energy Reports*, vol. 8, pp. 10 868–10 880, 2022. [Online]. Available: https://www.sciencedirect.com/science/article/pii/S2352484722016663

[17] A. Betz, "Das maximum der theoretisch moglichen auswendung des windes durch windmotoren," *Zeitschrift fur gesamte Turbinewesen*, vol. 26, pp. 1–300, 1920.

[18] J. T. Hansen, M. Mahak, and I. Tzanakis, "Numerical modelling and optimization of vertical axis wind turbine pairs: A scale up approach," *Renewable Energy*, vol. 171, pp. 1371–1381, 2021. [Online]. Available: https://www.sciencedirect.com/science/article/pii/S096014812100344X

[19] P. Lecanu and J. Breard, "Wind turbine with a vertical axis, particularly of the darrieus type," 2010, eP2183479.

[20] I. Robin, D. Mouazé, A.-C. Bennis, and G. Carpentier, "Evaluation of the overset method to assess the performances of an active lift turbine," *In review*, 2023.